



# A novel generalized strain hardening index (SHI) for long-chain branched polymer melts and its correlation to the steady-state compliance

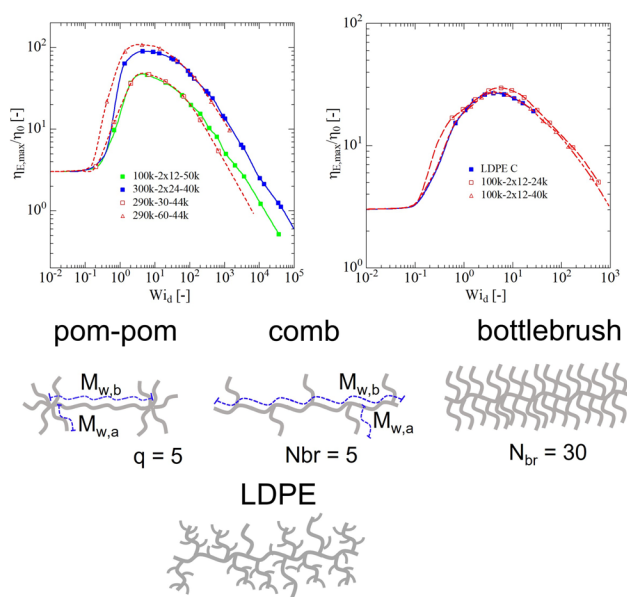
Manfred H. Wagner<sup>1</sup> · Max G. Schußmann<sup>2</sup> · Manfred Wilhelm<sup>2</sup> · Valerian Hirschberg<sup>2,3</sup>

Received: 25 April 2025 / Revised: 6 June 2025 / Accepted: 17 June 2025 / Published online: 4 August 2025  
 © The Author(s) 2025

## Abstract

Strain hardening of polymer melts in extensional flows is considered a desirable rheological feature because it stabilizes the homogeneity of free surface flows which is of importance, e.g., in film blowing, blow molding, and fiber spinning. Relating strain hardening to molecular characteristics, specifically topology in homopolymer melts, has been a long-standing challenge in rheology. While long-chain branching is known to be a decisive feature to enhance strain hardening, a general, quantitative relation between strain hardening and molecular topology is still missing. We propose a novel Strain Hardening Index (SHI) that can be used to assess the strain hardening behavior and to compare strain hardening of polymer melts with different topology and different chemistry, and we discuss its correlation with the steady-state compliance  $J_s^0$ . We consider the strain hardening characteristics of model polystyrene comb and pom-pom systems as well as of model poly((±)-lactide) graft copolymers and several polydisperse low-density polyethylene melts. We show that the proposed SHI of typical low-density polyethylene melts is equivalent to that of polystyrene pom-poms and combs with specific topologies. This finding might pave the way to rheologically informed topological tailoring of the strain hardening of industrially important polymers such as, e.g., polyethylene.

## Graphical Abstract



Extended author information available on the last page of the article

**Keywords** Elongational viscosity · Strain hardening · Branched topology · Comb polymers · Pom-pom polymers · Polylactides · Long-chain branched polyethylene · HMMSF model

## Introduction

Strain hardening of polymer melts in extensional flows is an important property for polymer processing because it stabilizes homogeneity of free surface flows such as, e.g., film blowing, blow molding, and fiber spinning. Relating strain hardening to molecular characteristics has been a long-standing challenge in rheology, but while long-chain branching (LCB) is known to be important to enhance strain hardening, a general, quantitative complete relation between strain hardening and a given molecular topology is still missing (Dealy et al. 2018). The quest for such a correlation has been hampered by two issues: (1) the lack of a broad variety of model polymers with well-defined branched topologies and (2) the lack of a method for the quantitative assessment of strain hardening enabling the comparison of different polymer systems investigated at different temperatures. The standard method of measuring strain hardening is via the strain hardening (SH) coefficient or strain hardening factor (SHF), i.e., by considering the ratio of the elongational stress growth coefficient  $\eta_E^+(t, \dot{\epsilon})$  to the linear-viscoelastic start-up viscosity  $\eta_E^0(t)$ :

$$SHF = \frac{\eta_E^+(t, \dot{\epsilon})}{\eta_E^0(t)} \quad (1)$$

Instead of  $\eta_E^0(t)$ , occasionally, the elongational stress growth coefficient  $\eta_E^{DE}(t, \dot{\epsilon})$  following from the Doi-Edwards (DE) tube model is used (Doi and F. Edwards 1978; Doi and Edwards 1979). The SHF depends on strain rate  $\dot{\epsilon}$  as well as time  $t$  resulting in a Hencky strain  $\epsilon = \dot{\epsilon}t$ ,

$$SHF = SHF(\epsilon, \dot{\epsilon}) \quad (2)$$

and is therefore temperature dependent and a function of the underlying relaxation time distribution. The SHF indicates the change of *transient* strain hardening with strain rate  $\dot{\epsilon}$  in start-up elongational flow at a prescribed Hencky strain  $\epsilon$  and at a particular experimental temperature for the specific polymer system considered, see, e.g., references (Münstedt 2023, 2024). However, as the SHF does not contain a characteristic material time constant, it cannot be used to compare the strain hardening potential of different polymer systems or at different temperatures. Another shortcoming of the SHF is its dependence on a specific Hencky strain  $\epsilon$ , which was dictated in the past by experimental limitations that did not permit reaching the steady-state elongational viscosity  $\eta_E(\dot{\epsilon})$  or, in the case of sample rupture or elongational stress

overshoot, the maximal elongational viscosity  $\eta_{E, \max}(\dot{\epsilon})$ . Improvements in elongational rheometry such as the Sentmanat extensional rheometer (SER), the extensional viscosity fixture (EVF), and the filament stretching rheometer (FSR) allow now in many cases to obtain a fair assessment of  $\eta_{E, \max}(\dot{\epsilon})$  (Huang 2022; Hirschberg et al. 2024). Using the Meissner-type elongational rheometer, Laun and Münstedt reported already in 1978 that strain hardening of a low-density polyethylene (LDPE) melt results in a steady-state elongational viscosity  $\eta_E(\dot{\epsilon})$  which first increases to values above the Trouton ratio  $\eta_E^0(\dot{\epsilon} \rightarrow 0)/\eta_0 = 3$  and after a maximum decreases with increasing elongation rate. Later, Münstedt and Laun (1981) used this maximum to distinguish and quantify the strain hardening of several LDPEs and found that strain hardening increases with increasing values of the steady-state compliance  $J_s^0$ . From a polymer processing point of view, we note that the effective elongational viscosity found in the so-called Rheotens tests resembles the steady-state elongational viscosity  $\eta_E(\dot{\epsilon})$  as far as the dependence on the strain rate is concerned, albeit on a lower viscosity level due to the effect of pre-straining in the extrusion die followed by free surface flow. Thus, using a measure of strain hardening derived from the steady-state elongational viscosity  $\eta_E(\dot{\epsilon})$  may have some advantage with respect to polymer processing over the SHF based on the transient elongational viscosity  $\eta_E^+(t, \dot{\epsilon})$ . Also, it would be of interest to verify and possibly explain the correlation of strain hardening of long-chain branched polymers with the steady-state compliance  $J_s^0$ .

Regarding the relation of strain hardening and molecular topology of branched polymers, recent progress in living anionic polymerization techniques has enabled the synthesis of well-defined model polystyrene (PS) polymer systems such as PS combs and pom-pom polymers in quantities allowing extensive elongational characterization (Wagner et al. 2004; Hepperle and Münstedt 2006; Nielsen et al. 2006; Kempf et al. 2010, 2013; Lentzakis et al. 2013; Abbasi et al. 2017, 2019; Faust et al. 2023; Hirschberg et al. 2023b, a; Zografos et al. 2023, 2024; Schußmann et al. 2024a, b). We have shown that the elongational viscosity of these systems is well described by the HMMSF (Narimissa et al. 2015; Narimissa and Wagner 2016, 2019a, b) or the EHMMMSF model (Wagner et al. 2022; Wagner and Hirschberg 2023) up to the steady-state elongational viscosity  $\eta_E(\dot{\epsilon})$  or in case of fracture, the maximal elongational viscosity  $\eta_{E, \max}(\dot{\epsilon})$ .

These models take into account hierarchical relaxation and dynamic dilution of the backbone by the side chains. In the following, we first consider  $\eta_{E, \max}(\dot{\epsilon})$  of monodisperse PS combs and monodisperse PS pom-poms as a function of the Weissenberg number  $Wi_d = \dot{\epsilon}\tau_d$  with the disengagement time  $\tau_d$  being a suitably defined material time constant. We show that the elongational viscosity  $\eta_{E, \max}(Wi_d)$  normalized by the zero-shear viscosity  $\eta_0$  is a useful measure to assess strain hardening, and we derive a novel strain hardening index (SHI). We discuss the effect of molecular topology, i.e., the effect of molecular weight of backbone and number as well as molecular weight of side chains on the strain hardening behavior. We then compare the strain hardening behavior of PS combs and pom-poms to the strain hardening of model poly(( $\pm$ )-lactide) graft copolymers (Wagner et al. 2024) as well as several polydisperse (commercial) LDPE melts (Wagner et al. 2022).

## Materials

The elongational rheology of a series of PS model combs of loosely to densely crafted combs to bottlebrushes (Fig. 1) was analyzed in Hirschberg et al. (2024). At constant backbone molecular weight  $M_{w,b}$  and with increasing number  $N_{br}$  of branches, the length of the backbone chain segment between two branch points of the comb decreases and the strain hardening increases. It was found (Hirschberg et al. 2024) that when the number  $N_b$  of arms per number  $z_{bb}$  of entanglements of the backbone, i.e.,  $N_b = N_{br}/z_{bb}$ , is larger

than one, the high branching density leads to additional hyperstretching. Hyperstretching refers to an enhanced increase of the elongational stress growth function compared to samples with  $N_b < 1$ . Table 1 summarizes  $M_{w,b}$ ,  $N_{br}$ , and  $N_b$ , as well as the total molecular weight  $M_w$  and the polydispersity  $M_w/M_n$  of the comb systems considered here. The combs are named after  $M_{w,b}-N_{br}-M_{w,a}$ . In addition, we will consider the strain hardening potential of binary blends consisting of 5 to 50 wt% of comb PS310k-100-15 k and a monodisperse linear polystyrene PS43k with  $M_w = 43$  kg/mol.

Another interesting system of bottlebrush polymers are copolymers with a poly(norbornene) backbone and one poly(( $\pm$ )-lactide) side chain with  $N_{sc} = 72$  repeat units and molecular weight  $M_w = 10.5$  kg/mol per two backbone repeating units (grafting density  $z = 0.5$ ). Above the star-to-bottlebrush transition at backbone degrees of polymerization of  $N_{bb} > 70$ , increasing strain hardening was observed with increasing  $N_{bb}$ , and their elongational rheology was recently investigated by Wagner et al. (2024). The molecular characteristics are summarized in Table 2.

In contrast to combs, a pom-pom polymer consists of a backbone chain of molecular weight  $M_{w,b}$  with two branch points at each end having  $q_a$  side arms of molecular weight  $M_{w,a}$  (Fig. 1). We consider here the elongational viscosity of a series of 12 pom-poms  $M_{w,b}-2xq_a-M_{w,a}$  as reported by Hirschberg et al. (2023b, a) and Schußmann et al. (2024a, b) comprising a wide range of  $M_{w,a}$ ,  $M_{w,b}$ , and  $q_a$  (Table 3).

The elongational rheology of model combs and pom-poms will be compared to the maximal elongational

**Fig. 1** Schematic representation of a pom-pom, comb, and bottlebrush polymer; see also Table 1 in [7]

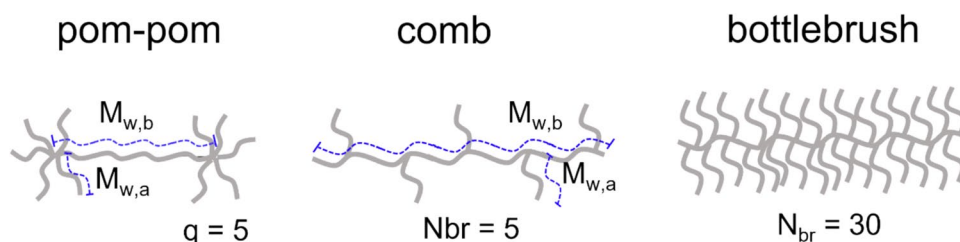


**Table 1** Molecular characteristics of PS combs. The number  $N_{br}$  of branches per entanglement length is based on entanglement molecular weight  $M_e = 14.5$  kg/mol

Combs	$M_{w,b}$ [kg/mol]	$N_{br}$ [-]	$N_b$ [-]	$M_{w,a}$ [kg/mol]	$M_w$ [kg/mol]	$M_w/M_n$ [-]
<b>Comb <math>M_{w,b}-N_{br}-M_{w,a}</math></b>						
PS290k-3-44 k	290	3	0.2	45	420	1.11
PS290k-10-44 k	290	10.4	0.5	44	750	1.15
PS290k-14-44 k	290	13.8	0.7	45	900	1.08
PS290k-30-44 k	290	29.8	1.6	43	1600	1.03
PS290k-60-44 k	290	59.5	3.0	44	2900	1.03
PS290k-120-44 k	290	120	6.0	44	5570	1.11
PS310k-100-40 k	310	100	4.7	40	4200	1.13
PS310k-100-15 k	310	100	4.7	15	1810	1.33

**Table 2** Molecular characterization of model poly((±)-lactide) graft copolymers: number of backbone repeating units  $N_{bb}$ , weight average molecular weight  $M_w$ , and polydispersity  $M_w/M_n$ . All graft copolymers have a grafting density per monomer unit in the backbone of  $z=0.5$  and the same number  $N_{sc}=72$  of side-chain (±)-lactide repeat units

Copolymer $N_{bb}$	$M_w$ [kg/mol]	$M_w/M_n$ [-]
Macromonomer ( $N_{sc}=72$ )	10.5	-
110	562	1.03
160	828	1.04
200	1080	1.04
320	1740	1.04
420	2240	1.18

viscosity of six commercial LDPE melts as already investigated by Wagner et al. (2022) and Wagner and Hirschberg (2023). The molecular characteristics of the LDPEs are summarized in Table 4.

## The hierarchical molecular stress function (HMMSF) model

We give a short summary of the basic equations of the hierarchical multi-mode molecular stress function (HMMSF) model (Narimissa and Wagner 2016, 2019a, b); for details, please refer to the original publications. The extra stress tensor is given by:

$$\sigma(t) = \sum_i \int_{-\infty}^t \frac{\partial G_i(t-t')}{\partial t'} f_i^2(t, t') \mathbf{S}_{DE}^{IA}(t, t') dt' \quad (3)$$

The relaxation modulus  $G(t)$  is expressed by a parsimonious spectrum of Maxwell modes with relaxation moduli  $g_i$  and relaxation times  $\tau_i$  (Poh et al. 2022):

$$G(t) = \sum_i G_i(t) = \sum_i g_i \exp(-t/\tau_i) \quad (4)$$

where  $\mathbf{S}_{DE}^{IA}$  is the Doi and Edwards (1978, 1979) strain tensor assuming independent alignment (IA) of tube segments with  $\mathbf{S}_{DE}^{IA} = 5\mathbf{S}$ , where  $\mathbf{S}$  is the second order orientation tensor. The molecular stress functions  $f_i = f_i(t, t')$  are inversely proportional to effective tube segments with diameters  $a_i$  representing each mode  $i$  and are functions of both the

**Table 3** Molecular characteristics of PS pom-poms

Pom-poms	$M_{w,b}$ [kg/mol]	$M_{w,b}/M_n$ [-]	$M_{w,a}$ [kg/mol]	$M_{w,a}/M_n$ [-]	$q_a$ [-]	$M_w$ [kg/mol]	$M_w/M_n$ [-]
<b>Pom-pom <math>M_{w,b}-2xq_a-M_{w,a}</math></b>							
100 k-2 × 12–24 k	100	1.05	24	1.05	2 × 12	600	1.18
100 k-2 × 12–40 k	100	1.05	40	1.08	2 × 12	1060	1.16
100 k-2 × 14–50 k	100	1.05	50	1.20	2 × 14	1500	1.27
100 k-2 × 22–25 k	100	1.05	25	1.15	2 × 22	1200	1.15
220 k-2 × 9–25 k	220	1.06	25	1.08	2 × 9	670	1.08
220 k-2 × 10–40 k	220	1.06	40	1.10	2 × 10	1020	1.09
280 k-2 × 22–22 k	280	1.04	22	1.07	2 × 22	1248	1.15
400 k-2 × 9–23 k	400	1.10	23	1.14	2 × 9	814	1.15
400 k-2 × 13–40 k	400	1.10	40	1.15	2 × 13	1360	1.15
300 k-2 × 24–40 k	300	1.40	40	1.03	2 × 24	2220	1.40
100 k-2 × 5–25 k	100	1.05	25	1.05	2 × 5	350	1.12
220 k-2 × 3–70 k	220	1.06	70	1.04	2 × 3	640	1.11

**Table 4** Characterization of LDPE melts

Characteristics	LDPE A	LDPE B	LDPE C	DOW150R	1840H-V	3020D
Producer	Dow	Dow	Dow	Dow	BASF	BASF
$M_w$ [kg/mol]	160	320	180	242	89	300
$M_w/M_n$	11	22	15	11	4	8
$\rho$ at $rt$ [g/cm <sup>3</sup> ]	0.920	0.919	0.918	0.921	0.920	0.94
$MFR$ [g/10 min]	2.0	8.5	3.9	0.18	-	-
$Ea$ [kJ/mol]	65	65	65	-	-	64

observation time  $t$  (the time when the stress is measured) and the time  $t'$  of creation of tube segments by diffusion. Hierarchical relaxation and dynamic dilution of tube segments are already contained in the linear-viscoelastic relaxation spectrum, and the effect of dilution by hierarchical relaxation can be extracted from the spectrum. We distinguish between the regime of permanent dilution and the regime of dynamic dilution. The presence of oligomeric chains and unentangled (fluctuating) chain ends leads to permanent dilution, while dynamic dilution starts as soon as the relaxation process reaches the dilution modulus  $G_D \leq G_N^0$ . The dilution modulus  $G_D$  is a free parameter of the model, which is fitted to the non-linear viscoelastic experimental data. Dynamic dilution starts at time  $t = \tau_D$ , when the relaxation modulus  $G(t)$  has relaxed to the value of  $G_D$ , while at times  $t \leq \tau_D$ , the chain segments are assumed to be permanently diluted. The fraction  $w_i$  of dynamically diluted polymer segments of mode  $i$  with relaxation time  $\tau_i > \tau_D$  is determined by the ratio of the relaxation modulus at time  $t = \tau_i$  to the dilution modulus  $G_D$ :

$$w_i^2 = \frac{G(t = \tau_i)}{G_D} = \frac{1}{G_D} \sum_{j=1}^n g_j \exp(-\tau_i/\tau_j) \quad \text{for } \tau_i > \tau_D \quad (5)$$

$$w_i^2 = 1 \quad \text{for } \tau_i \leq \tau_D$$

The value of the volume fraction  $w_i$  at  $t = \tau_i$  is attributed to the chain segments with relaxation time  $\tau_i$ . Segments with  $\tau_i < \tau_D$  are considered permanently diluted, and their volume fractions are assumed to be equal to 1.

Restricting attention to comb and pom-pom polymers in extensional flows and accounting for the effects of stretch relaxation, the evolution equation for the molecular stress function  $f_i$  of each mode  $i$  can be expressed as (Hirschberg et al. 2024)

$$\frac{\partial f_i}{\partial t} = (1 + k)f_i(\mathbf{K} : \mathbf{S}) - \frac{f_i - 1}{\tau_i}(1 - w_i^2) - \frac{(f_i^5 - 1)}{5\tau_i}w_i^2 \quad (6)$$

with the initial conditions  $f_i(t = t', t') = 1$ . The first term on the right hand side represents the hyperstretching rate with  $0 \leq k \leq 1$ ; the second term takes into account stretch relaxation, and the third term limits stretch due to enhanced relaxation of stretch on smaller length scales, leading to a stretch relaxation term which is proportional to the 5th power of the stretch  $f_i$ .

In elongational flow of polymer samples showing strong transient strain hardening, brittle or elastic fracture at higher strain rates is frequently observed (Huang et al. 2016; Huang and Hassager 2017). According to the entropic fracture hypothesis (Wagner et al. 2021, 2022; Hirschberg et al. 2023a; Wagner and Hirschberg 2023), fracture will occur when the strain energy of a chain segment reaches the bond energy  $U$  of a carbon–carbon bond. Due to thermal

fluctuations, the total strain energy of the chain segment will be concentrated for a short time on one C–C bond by thermal fluctuations, consequently leading to rupture of a covalent bond. This leads to crack initiation and within a few milliseconds to macroscopic fracture. The critical stretch  $f_{i,c}$  at fracture is given by

$$f_{i,c} = \sqrt{\frac{U}{3k_B T w_i}} \quad (7)$$

with  $k_B$  being the Boltzmann constant and  $T$  the absolute temperature. The ratio of bond-dissociation energy  $U$  to thermal energy  $3k_B T$  is approximately  $U/3k_B T = 32$  and 31 at temperatures of  $T = 160^\circ\text{C}$  and  $180^\circ\text{C}$ , respectively. This fracture criterion has been shown to be in agreement with experimental evidence of polymer melts and solutions, and the general energy to break a single C–C bond, see e.g., Hirschberg et al. (2023b, a), Poh et al. (2023), and Wagner and Hirschberg (2024).

Thus, the HMMSF model for LCB polymer melts consists of the multi-mode stress (Eq. (3)), a set of evolution equations for the molecular stress functions  $f_i$  (Eq. (6)), and a hierarchical procedure to quantify the fraction of dynamically diluted chain segments according to Eq. (5) with two free nonlinear parameters, the dilution modulus  $G_D$  and the hyperstretch factor  $k$ . Once the linear-viscoelastic relaxation spectrum of a polydisperse polymer melt is known, the weight fractions  $w_i$  in the evolution (Eq. (5)) can be obtained by fitting the value of  $G_D$  to the elongational viscosity. The parameter  $G_D$ , in conjunction with the hyperstretch factor  $k$  (see Eq. 6), determines the extent of strain hardening. These two free parameters are sufficient for modeling extensional flows of LCB polymers. For the comb and pom-pom polymers of Tables 1 and 3 with many side arms, the dilution modulus  $G_D$  is equal to the plateau modulus  $G_N^0$ , i.e., dynamic dilution starts right at the plateau modulus. We also note that the hyperstretch factor is zero for the pom-pom polymers considered, and therefore, in the case of the pom-poms, the HMMSF model does not depend on any free parameter.

## The strain hardening index (SHI)

As we will show in the following, the Strain Hardening Index (SHI) depends on the product of two terms, one depending on the linear-viscoelastic (LVE) characterization of the melt in terms of the relaxation modulus  $G(t)$  (Eq. (4)), the other being a characteristic measure of stretch of chain segments. From the 1st and 2nd moment of the parsimonious relaxation time spectrum, the zero-shear viscosity  $\eta_0$ , the viscosity average relaxation time  $\tau_v$ , the disengagement time  $\tau_d$ , and the steady-state compliance  $J_s^0$  are obtained by



$$\eta_0 = \sum_i g_i \tau_i \quad (8a)$$

$$\tau_v = \frac{\eta_0}{G_N^0} \quad (8b)$$

$$\tau_d = \frac{\sum_i g_i \tau_i^2}{\eta_0} \quad (8c)$$

$$J_s^0 = \frac{\sum_i g_i \tau_i^2}{\eta_0^2} \quad (8d)$$

While  $\tau_d$  is an aggregated measure of the long-time part of the relaxation time spectrum,  $J_s^0$  determines the recoverable deformation or “elasticity” in the LVE regime, and with  $J_s^0 G_N^0 = \tau_d / \tau_v$ , it is also a measure of the broadness of the relaxation time spectrum.

To elucidate the essence of strain hardening, we simplify the HMMSF model to a one-mode model with relaxation time  $\tau_d$  and modulus  $G_d$ , which is the value of the relaxation modulus  $G(t)$  at time  $t = \tau_d$ :

$$G_d = G(t = \tau_d) \quad (9)$$

Thus,  $\tau_d$  and  $G_d$  are representative quantities of the long-time part of the relaxation time spectrum relevant for stretching. The stress tensor (Eq. (3)) then simplifies to

$$\sigma(t) = \int_{-\infty}^t G_d / \tau_d \exp[-(t - t') / \tau_d] f^2(t, t') \mathbf{S}_{DE}^{IA}(t, t') dt' \quad (10)$$

and the evolution of stretch (Eq. (5)) to

$$\frac{\partial f}{\partial t} = (1 + k)f(\mathbf{K} : \mathbf{S}) - \frac{f - 1}{\tau_d}(1 - w_d^2) - \frac{(f^5 - 1)}{5\tau_d} w_d^2 \quad (11)$$

$w_d$  is the dynamically diluted polymer fraction:

$$w_d = (G_d / G_D)^{1/2} \quad (12)$$

In fast elongational flow and large values of  $Wi_d = \dot{\epsilon} \tau_d$ , the elongational stress is obtained from Eq. (10) as

$$\sigma_E(Wi_d) \cong 5f^2(Wi_d)G_d \quad (13)$$

and at large Hencky strain, the square of the steady-state stretch  $f^2(Wi_d)$  is obtained from Eq. (11) as

$$f^2(Wi_d) \cong \frac{1}{w_d} \sqrt{5(1 + k)Wi_d} \quad (14)$$

From Eq. (13), the elongational viscosity is then given by  $\eta_E(Wi_d) = \frac{\sigma_E(Wi_d)}{\dot{\epsilon}} = \frac{\sigma_E(Wi_d)\tau_d}{Wi_d}$ . Normalized by the zero-shear viscosity  $\eta_0$ , this results in

$$\frac{\eta_E(Wi_d)}{\eta_0} \cong 5f^2(Wi_d) \frac{G_d \tau_d / \eta_0}{Wi_d} = \frac{5}{w_d} \sqrt{5(1 + k)Wi_d} \frac{G_d J_s^0}{Wi_d} \quad (15)$$

From the right-hand side of this equation, we see that  $\eta_E(Wi_d)$  decreases with increasing  $Wi_d$  according to  $\eta_E(Wi_d) \propto Wi_d^{-1/2}$ , and we note that this relation is often observed experimentally. We define the strain hardening index (SHI) as the normalized elongational viscosity  $\eta_E(Wi_d) / \eta_0$  taken heuristically at  $Wi_d = 1$ ,

$$SHI = \frac{\eta_E(Wi_d = 1)}{\eta_0} \cong 5f_d^2 G_d J_s^0 \quad (16)$$

with the square of the characteristic stretch

$$f_d^2 = f^2(Wi_d = 1) = \frac{1}{w_d} \sqrt{5(1 + k)} = \sqrt{5(1 + k) \frac{G_D}{G_d}} \quad (17)$$

While the term  $5G_d J_s^0$  in Eq. (16) is determined by the LVE characterization of the melt, the characteristic stretch  $f_d$  depends on dynamic dilution according to Eq. (12) and to a minor part on the hyperstretch factor  $k$ . We note that the SHI is inherently temperature-independent, at least for thermorheologically simple materials.

## Comparison of strain hardening of different polymer systems

Figure 2 shows the maximal value of the normalized elongational viscosity  $\eta_{E,\max} / \eta_0$  corresponding to the steady-state elongational viscosity or the maximal elongational viscosity reached in the case of fracture, as a function of Weissenberg number  $Wi_d = \dot{\epsilon} \tau_d$  for the series of model PS combs (Table 1). Lines are calculated by the use of the HMMSF model, and symbols indicate the calculated values at the experimentally investigated strain rates. Because model and experimental data agree quantitatively (Hirschberg et al. 2023b, a, 2024), the symbols also represent the maximal elongational viscosities reached experimentally. The elongational viscosity of all comb systems has a similar shape, and  $\eta_{E,\max} / \eta_0$  first increases and, after reaching a maximum at  $3 \leq Wi_d \leq 8$ , decreases with increasing  $Wi_d$ . We designate the observed maximal value of the reduced elongational viscosity  $\eta_{E,\max}(Wi_d) / \eta_0$  as  $SHI_m$ :

$$SHI_m = \text{Max} \left[ \frac{\eta_{E,\max}(Wi_d)}{\eta_0} \right] \quad (18)$$

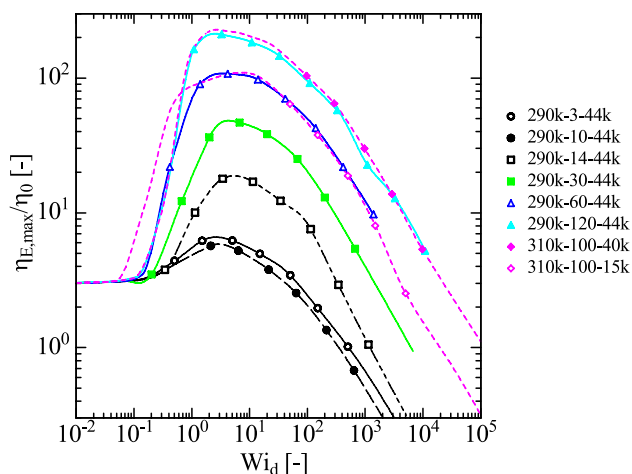


**Fig. 2** Normalized maximal elongational viscosity  $\eta_{E,max}/\eta_0$  as a function of Weissenberg number  $Wi_d = \dot{\epsilon}\tau_d$  for PS model combs  $M_{w,b}-N_{br}-M_{w,a}$ . Lines are calculated by the HMMSF model. Symbols indicate the calculated values at the experimental strain rates

As shown in Table 5,  $SHI_m$  is the higher, the larger is the number  $N_{br}$  of branches. It increases from  $SHI_m = 6.5$  for comb 290 k-3-44 k with 3 branches to  $SHI_m = 204$  for comb 290 k-120-44 k with 120 branches. Comb 310 k-100-40 k shows a slightly larger strain hardening potential with  $SHI_m = 227$  than comb 290 k-120-44 k, while  $\eta_{E,max}(Wi_d)/\eta_0$  of the combs 290 k-60-44 k (measured at 180 °C) and 310 k-100-15 k (measured at 160 °C) are nearly indistinguishable. There seems to exist a trade-off between number (60 versus 100) and length (44 k versus 15 k) of side chains. As seen from Table 5, while the zero-shear viscosity  $\eta_0$  and the disengagement time  $\tau_d$  change inconsistently with number  $N_{br}$  of branches, first increasing, then decreasing and increasing again, the steady-state compliance  $J_s^0$  increases consistently with increasing  $N_{br}$  of the combs with backbone molecular weight of 290 kg/

mol. It is interesting to note that the characteristic LVE term  $5G_dJ_s^0$  is of order 1, decreasing slightly with increasing  $J_s^0$ . For  $N_{br} \geq 30$ , i.e., when the number of branches per entanglement length of the backbone is larger than 1 (see Table 1), the dilution modulus  $G_D$  is equal to the plateau modulus  $G_N^0$ , and the hyperstretch factor  $k$  is larger than zero. The strain hardening index (SHI) calculated by Eq. (16) shows the same tendency as the experimentally observed  $SHI_m$  and is in nearly quantitative agreement with  $SHI_m$  up to  $SHI \approx 100$ , while at higher  $SHI$ ,  $SHI_m > SHI$  (Table 5). Nevertheless, it is remarkable that this level of agreement can be achieved by a single-mode approximation of the full HMMSF model.

The strain hardening potential of binary blends of PS comb 310 k-100-15 k and linear PS 43 k is presented in Fig. 3. Interestingly, strain hardening of the 50/50 blend as well as of the blend with only 5% of comb 310 k-100-15 k is indistinguishable from that of the pure comb 310 k-100-15 k, while the blends with 20% and 10% of comb 310 k-100-15 k show enhanced strain hardening in agreement with high values of  $J_s^0$  (Table 6). Thus, blending of comb 310 k-100-15 k with 80–90% of linear PS 43 k broadens the relaxation time spectrum drastically. Indeed, the reduced elongational viscosity and the strain hardening of these blends are within experimental accuracy identical to the strain hardening of the pure combs 290 k-100-44 k and 310 k-100-40 k, as shown in Fig. 4.

For the 12 model PS pom-pom melts of Table 3, the normalized elongational viscosity  $\eta_{E,max}/\eta_0$  as a function of Weissenberg number  $Wi_d = \dot{\epsilon}\tau_d$  is shown in Fig. 5. In contrast to the model PS combs investigated, pom-poms do not show hyperstretching even in the case of many side arms, and therefore,  $k = 0$ . Limited strain hardening is observed for pom-poms having only a few side arms at the two branched points such as 220 k-2 × 3-70 k ( $SHI_m = 6$ )

**Table 5** Characteristics of PS combs: weight fraction  $\phi_b$  of backbone, hyper stretch factor  $k$ , plateau modulus  $G_N^0$ , dilution modulus  $G_D$ , relaxation modulus  $G_d$ , zero-shear viscosity  $\eta_0$ , disengagement

Comb	$\phi_b$ [-]	$k$ [-]	$G_N^0$ [kPa]	$G_D$ [kPa]	$G_d$ [kPa]	$\eta_0$ [kPa s]	$\tau_d$ [s]	$J_s^0$ [kPa <sup>-1</sup> ]	$5G_dJ_s^0$ [-]	$w_d$ [-]	$f_d^2$ [-]	SHI [-]	SHI <sub>m</sub> [-]
PS290k-3-44 k	0.69	0	200	5	1.29	344	50.3	0.15	0.94	0.51	4.41	4.15	6.5
PS290k-10-44 k	0.40	0	220	5	2.03	1920	213	0.11	1.12	0.64	3.51	3.94	5.8
PS290k-14-44 k	0.32	0	210	80	1.61	751	114	0.15	1.22	0.14	15.8	19.3	19
PS290k-30-44 k	0.18	0.2	250	250	0.83	241	67.0	0.28	1.16	$5.8 \times 10^{-2}$	42.4	49.1	47
PS290k-60-44 k	0.10	0.5	210	210	0.092	89	139	1.56	0.72	$2.1 \times 10^{-2}$	131	93.8	106
PS290k-120-44 k	0.05	0.6	250	250	0.019	170	1091	5.53	0.52	$8.7 \times 10^{-3}$	326	170	204
PS310k-100-40 k	0.07	0.6	220	220	0.018	139	971	6.97	0.63	$9.1 \times 10^{-3}$	311	197	227
PS310k-100-15 k	0.17	0.6	320	320	0.17	550*	500*	0.91	0.75	$2.3 \times 10^{-2}$	125	93.3	109

\* $T = 160$  °C

time  $\tau_d$ , steady-state compliance  $J_s^0$ , diluted fraction  $w_d$ , square of representative stretch  $f_d^2$ , strain hardening index (SHI) (Eq. (16)), and observed strain hardening index ( $SHI_m$ ) for PS combs at  $T = 180$  °C

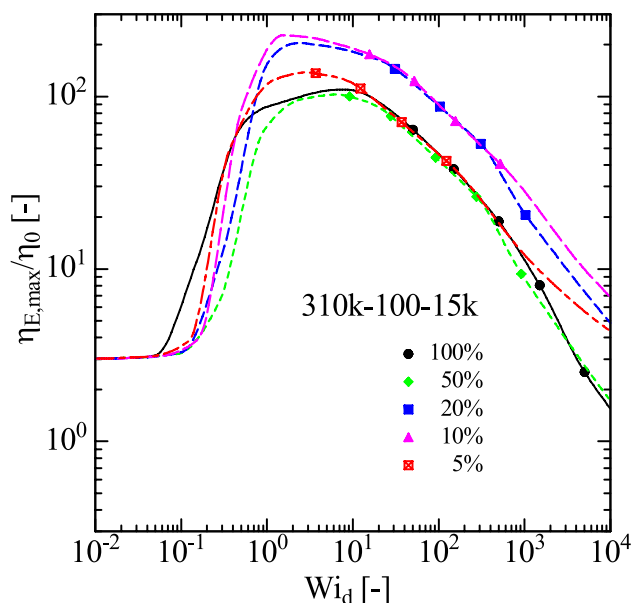


**Fig. 3** Normalized maximal elongational viscosity  $\eta_{E,max}/\eta_0$  as a function of Weissenberg number  $Wi_d = \dot{\epsilon}\tau_d$  for binary blends of PS comb 310 k-100-15 k (concentration given in wt%) and linear PS 43 k. Lines are calculated by the HMMSF model. Symbols indicate the calculated values at the experimental strain rates

and 100 k-2 × 5–25 k ( $SHI_m = 10$ ), irrespective of the length of the side arms. On the other hand, pom-pom 300 k-2 × 24–40 k with many side arms and the largest value of  $J_s^0$  shows the highest strain hardening potential with  $SHI_m = 90$ . Most of the other pom-poms fall in a narrow band with  $SHF_m \approx 30$ . Surprisingly, there is only a minor increase of  $SHF_m$  with increasing backbone molecular weight  $M_{w,b}$  from 100 to 400 kg/mol having a similar numbers of arms ( $q_a = 10$ –13) and the same side arm molecular weight of  $M_{w,a} = 40$  kg/mol (Fig. 6). Increasing the molecular weight of the side arms from 24 to 40 kg/mol at constant molecular weight of  $M_{w,b} = 100$  kg/mol and  $q_a = 12$  does not change strain hardening significantly, but a further increase of  $M_{w,a}$  to 50 kg/mol increases  $SHF_m$  to 47 (Fig. 7). We note that for  $M_{w,a} = 50$  kg/mol, the combined

molecular weight  $2M_{w,a}$  of two side arms is equal to the backbone molecular weight of  $M_{w,b} = 100$  kg/mol with the consequence that the entanglements of the arms act in a similar way as the entanglements of the backbone, thereby broadening the relaxation time spectrum and thus increasing the value of the steady-state compliance  $J_s^0$  significantly. We may consider pom-pom 100 k-2 × 14–50 k as a generalized H-polymer. As seen from Table 7,  $5G_dJ_s^0$  is again of order 1 for all pom-poms investigated and there is general agreement of observed  $SHI_m$  and the strain hardening index (SHI) calculated from Eq. (16).

In Fig. 8, the normalized maximal elongational viscosity  $\eta_{E,max}(Wi_d)/\eta_0$  of the two model pom-poms featuring the highest strain hardening potentials of all pom-poms investigated, 100 k-2 × 12–50 k and 300 k-2 × 24–40 k, is compared to that of combs 290–30–44 k and 290–60–44 k. We may conclude that if total number of side arms  $2q_a$  of the pom-poms is roughly similar to the number  $N_{br}$  of side branches of the combs, specifically  $N_{br} = 30$  and  $2q_a = 24$  for comb 290–30–44 k and pom-pom 100 k-2 × 12–50 k, respectively;  $N_{br} = 60$  and  $2q_a = 48$  for comb 290–60–44 k and pom-pom 300 k-2 × 24–40 k, respectively, the strain hardening behavior is similar, and the exact location of the arms within the macromolecule has only a minor effect.

We now consider the strain hardening of polymers of a different chemistry, namely of bottlebrush copolymers with a poly(norbornene) backbone of polymerization degree of  $N_{bb} = 100$  to 420 and one poly((±)-lactide) side chain per two backbone repeat units (grafting density per backbone monomer  $z = 0.5$ ) (Table 2). As shown in Fig. 9, the normalized maximal elongational viscosity  $\eta_{E,max}/\eta_0$  as a function of Weissenberg number  $Wi_d = \dot{\epsilon}\tau_d$  increases with increasing  $N_{bb}$  in agreement with the increasing value of  $J_s^0$  (Table 8) and reaches maximal values at  $Wi_d = 3$ –5. Again, there is good agreement of observed  $SHI_m$  and the strain hardening index (SHI) calculated from Eq. (16). Comparison of  $\eta_{E,max}(Wi_d)/\eta_0$  of the PLA bottlebrushes to PS combs 290 k-30–44 k and 290 k-14–44 k is also shown in Fig. 9. The strain hardening of the PLA bottlebrush with  $N_{bb} = 420$  is slightly higher than that of PS comb 290 k-30–44 k, while

**Table 6** Characteristics of binary blends of PS comb 310 k-100-15 k and linear PS 43 k: weight fraction  $\phi_b$  of backbone, hyper stretch factor  $k$ , plateau modulus  $G_N^0$ , dilution modulus  $G_D$ , relaxation modulus  $G_d$ , zero-shear viscosity  $\eta_0$ , disengagement time  $\tau_d$ , steady-state com-

pliance  $J_s^0$ , diluted fraction  $w_d$ , square of representative stretch  $f_d^2$ , strain hardening index (SHI) (Eq. (16)), and experimentally determined strain hardening index ( $SHI_m$ ) for binary blends of PS comb 310 k-100-15 k and linear PS43k at  $T = 160$  °C

Comb	$\phi_b$ [-]	$k$ [-]	$G_N^0$ [kPa]	$G_D$ [kPa]	$G_d$ [kPa]	$\eta_0$ [kPa s]	$\tau_d$ [s]	$J_s^0$ [kPa <sup>-1</sup> ]	$5G_dJ_s^0$ [-]	$w_d$ [-]	$f_d^2$ [-]	SHI [-]	$SHI_m$ [-]
100% PS310k-100-15 k	0.17	0.6	320	320	0.17	550	500	0.91	0.75	$2.3 \times 10^{-2}$	125	93.3	109
50% PS310k-100-15 k	0.09	0.6	180	180	0.13	66.3	91.9	1.39	0.87	$2.6 \times 10^{-2}$	107	93.1	100
20% PS310k-100-15 k	0.03	0.6	200	200	0.015	15.9	103	6.49	0.48	$8.6 \times 10^{-3}$	329	158	204
10% PS310k-100-15 k	0.02	0.6	160	160	0.0074	4.95	52.2	10.5	0.39	$6.8 \times 10^{-3}$	416	162	223
5% PS310k-100-15 k	0.01	0.6	200	200	0.040	4.79	12.3	2.57	0.52	$1.4 \times 10^{-2}$	200	103	136



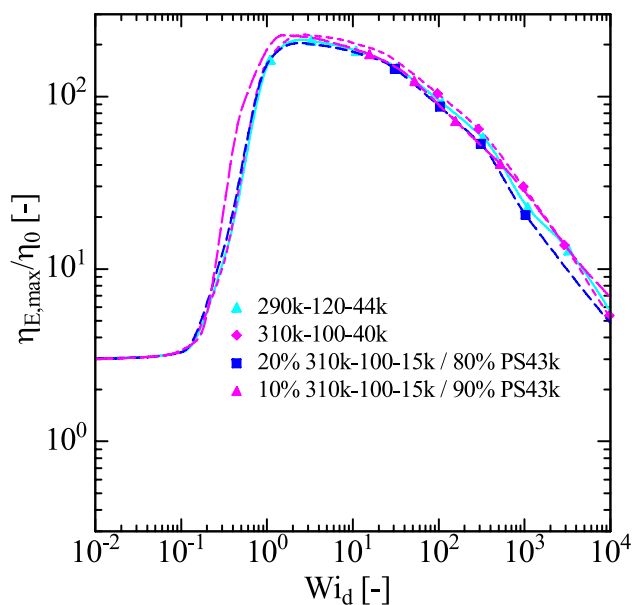


**Fig. 4** Comparison of normalized maximal elongational viscosity  $\eta_{E,max}(Wi_d)/\eta_0$  of combs 290 k-120-44 k and 310 k-100-40 k to binary blends of 20% and 10% PS comb 310 k-100-15 k and linear PS 43 k. Lines are calculated by the HMMSF model. Symbols indicate the calculated values at the experimental strain rates

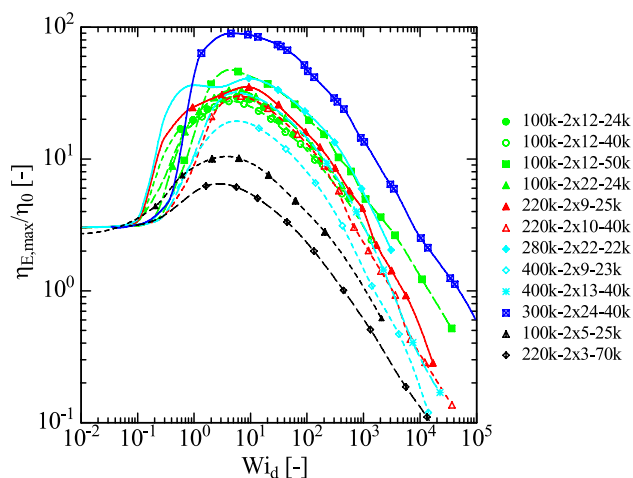


**Fig. 5** Normalized maximal elongational viscosity  $\eta_{E,max}/\eta_0$  as a function of Weissenberg number  $Wi_d = \dot{\epsilon}\tau_d$  for PS model pom-poms  $M_{w,b}-2xq_a-M_{w,a}$ . Lines are calculated by the HMMSF model. Symbols indicate the calculated values at the experimental strain rates

the strain hardening for  $N_{bb}=200$  corresponds to that of comb 290 k-14-44 k. From this comparison, we may conclude that strain hardening is correlated with the number of side chains, irrespective of the length of the backbone: While the PLA bottlebrush  $N_{bb}=420$  and the PS comb 290 k-30-44 k have about twice as many side chains as bottlebrush  $N_{bb}=200$  and comb 290 k-14-44 k, respectively, the

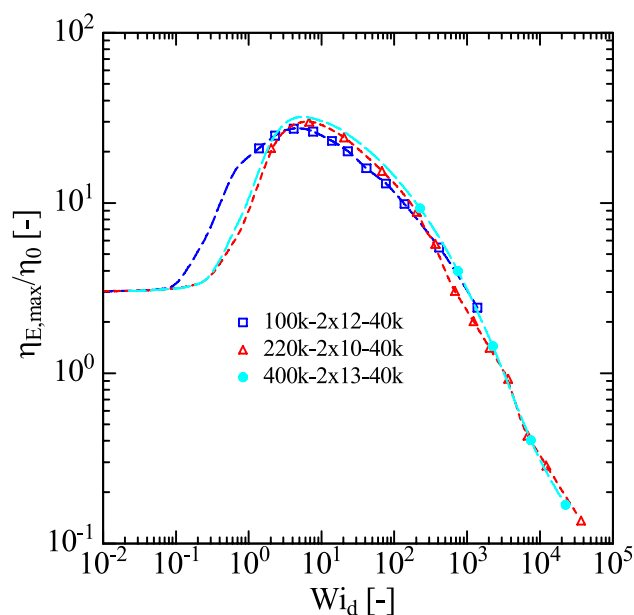


**Fig. 6** Normalized maximal elongational viscosity  $\eta_{E,max}(Wi_d)/\eta_0$  for PS model pom-poms with different  $M_{w,b}$  but same  $M_{w,a}=40$  kg/mol and  $q_a=10-13$

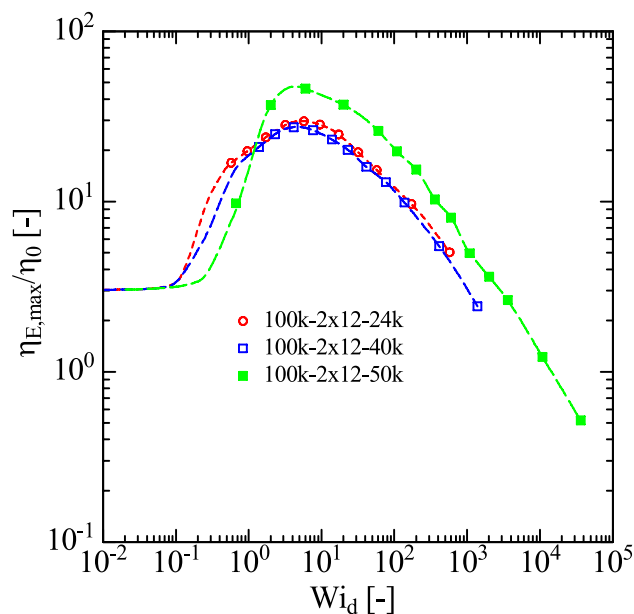


**Fig. 7** Normalized maximal elongational viscosity  $\eta_{E,max}(Wi_d)/\eta_0$  for PS model pom-poms with  $M_{w,b}=100$  and  $q_a=12$ , but different  $M_{w,a}$

backbone length of the two combs is the same ( $M_w=290$  k), but the backbone length of bottlebrush  $N_{bb}=420$  is more than twice the length of  $N_{bb}=200$ .

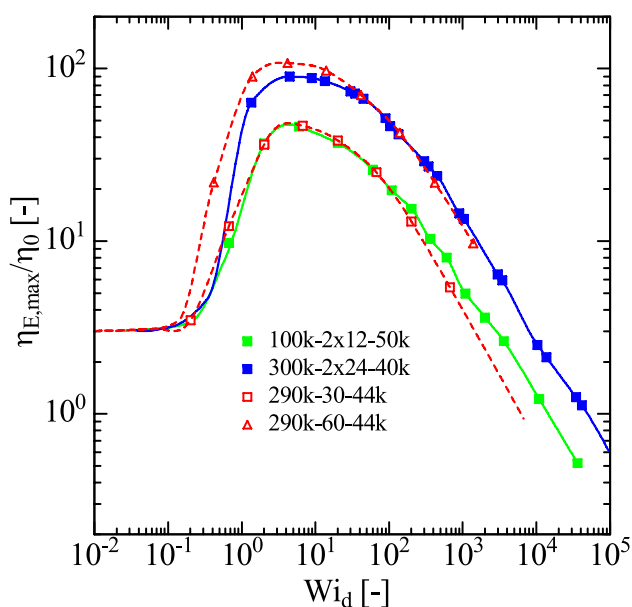
The normalized elongational viscosity  $\eta_{E,max}/\eta_0$  as a function of Weissenberg number  $Wi_d = \dot{\epsilon}\tau_d$  for the 6 LDPE melts of Table 4 and measured at temperatures between

**Table 7** Characteristics of PS pom-poms: weight fraction  $\phi_b$  of backbone, plateau modulus  $G_N^0$ , dilution modulus  $G_D$ , relaxation modulus  $G_d$ , zero-shear viscosity  $\eta_0$ , disengagement time  $\tau_d$ , steady-state com-

pliance  $J_s^0$ , diluted fraction  $w_d$ , square of representative stretch  $f_d^2$ , strain hardening index (SHI) (Eq. (16)), and observed strain hardening index (SHI<sub>m</sub>) for PS pom-poms at  $T = 160^\circ\text{C}$

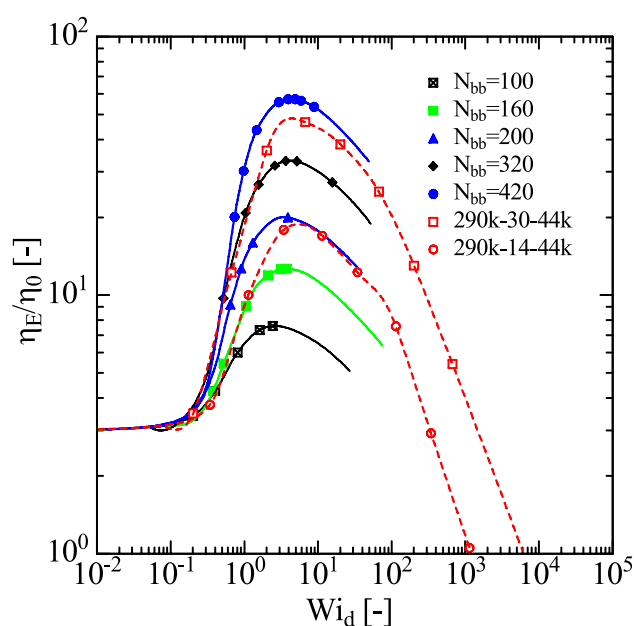
Pom-pom	$\phi_b$ [-]	$G_N^0$ [kPa]	$G_D$ [kPa]	$G_d$ [kPa]	$\eta_0$ [kPa s]	$\tau_d$ [s]	$J_s^0$ [kPa <sup>-1</sup> ]	$5G_d J_s^0$ [-]	$w_d$ [-]	$f_d^2$ [-]	SHI [-]	SHI <sub>m</sub> [-]
100 k-2×12–24 k	0.15	270	270	1.75	26	3.18	0.12	1.05	$8.0 \times 10^{-2}$	27.8	29.3	30
100 k-2×12–40 k	0.09	190	190	1.45	56	7.67	0.14	1.00	$8.7 \times 10^{-2}$	25.6	25.5	27
100 k-2×14–50 k	0.07	110	110	0.21	220	201	0.90	0.93	$4.4 \times 10^{-2}$	51.4	48.0	47
100 k-2×22–25 k	0.09	310	310	1.54	17	2.29	0.14	1.05	$7.0 \times 10^{-2}$	31.7	33.2	33
220 k-2×9–25 k	0.33	260	260	1.05	$1.5 \times 10^3$	313	0.21	1.11	$6.4 \times 10^{-2}$	35.1	39.1	35
220 k-2×10–40 k	0.22	190	190	1.46	$3.5 \times 10^3$	679	0.19	1.42	$8.8 \times 10^{-2}$	25.5	36.2	31
280 k-2×22–22 k	0.22	290	290	0.39	830	308	0.37	0.71	$3.6 \times 10^{-2}$	61.3	43.7	41
400 k-2×9–23 k	0.49	170	170	3.60	$1.9 \times 10^4$	1406	0.07	1.32	$1.5 \times 10^{-1}$	15.4	20.3	19
400 k-2×13–40 k	0.28	190	190	1.16	$3.5 \times 10^4$	7512	0.21	1.22	$7.8 \times 10^{-2}$	28.7	35.1	34
300 k-2×24–40 k	0.14	150	150	0.039	$1.0 \times 10^3$ *	3441*	3.35	0.64	$1.6 \times 10^{-2}$	140	90.1	90
100 k-2×5–25 k	0.29	180	40	3.67	330*	20.8*	0.06	1.15	$3.0 \times 10^{-1}$	7.38	8.46	10
220 k-2×3–70 k	0.34	190	3	0.99	$3.0 \times 10^5$ *	70,945*	0.23	1.32	$5.7 \times 10^{-1}$	3.40	4.50	6

\* $T = 140^\circ\text{C}$



**Fig. 8** Comparison of normalized maximal elongational viscosity  $\eta_{E,\max}(Wi_d)/\eta_0$  of PS model pom-poms 100 k-2×12–50 k and 300 k-2×24–40 k to PS combs 290–30–44 k and 290–60–44 k

130 and 160 °C is presented in Fig. 10. Except for LDPE B, the LDPE melts show elongational stress overshoot in startup elongational flow (Wagner et al. 2022). The maximal elongational viscosity  $\eta_{E,\max}/\eta_0(Wi_d)$  is therefore taken as the maximum of  $\eta_E^+(t, Wi_d)$ . LDPE B with the highest polydispersity shows the highest strain hardening with a peak of  $\text{SHI}_m = 30$  at  $Wi_d \approx 2$ , while LDPE 3020D with the highest room temperature density of  $\rho_{RT} = 0.94\text{g/cm}^3$ , and therefore, the smallest amount of branching has the lowest

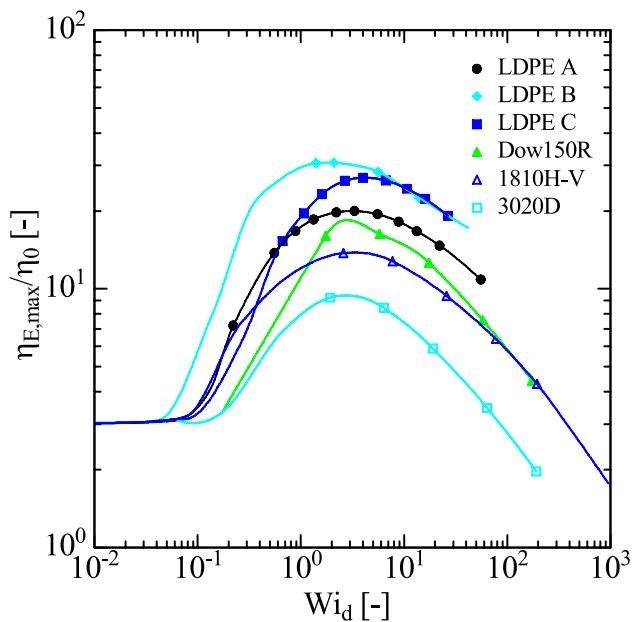


**Fig. 9** Normalized maximal elongational viscosity  $\eta_{E,\max}/\eta_0$  as a function of Weissenberg number  $Wi_d = \dot{\epsilon}\tau_d$  for PLA bottlebrushes with different number  $N_{bb}$  of backbone repeat units at constant graft density  $z = 0.5$  and the same number  $N_{sc} = 72$  of side-chain ( $\pm$ )-lactide repeat units, and comparison to PS combs 290 k-30–44 k and 290 k-14–44 k. Lines are calculated by the HMMSF model. Symbols indicate the calculated values at the experimental strain rates

strain hardening index of  $\text{SHI}_m = 9$  at  $Wi_d \approx 3$  (Table 9). Comparison of  $\eta_{E,\max}/\eta_{0d}(Wi_d)$  of LDPE A, B, and C to PS combs 290 k-30–44 k and 290 k-14–44 k is shown in Fig. 11. Due to the broad molecular weight distribution of the LDPE melts,  $\eta_{E,\max}/\eta_{0d}(Wi_d)$  starts to increase already

**Table 8** Characteristics of poly((±)-lactide) (PLA) graft copolymers: weight fraction  $\phi_b$  of backbone, plateau modulus  $G_N^0$ , dilution modulus  $G_D$ , relaxation modulus  $G_d$ , zero-shear viscosity  $\eta_0$ , disengagement time  $\tau_d$ , steady-state compliance  $J_e^0$ , diluted fraction  $w_d$ , squareof representative stretch  $f_d^2$ , strain hardening index (SHI) (Eq. (16)), and observed strain hardening index (SHI<sub>m</sub>) for PLA bottlebrushes at  $T = 100^\circ\text{C}$ 

PLA	$\phi_b$ [-]	$k$ [-]	$G_N^0$ [kPa]	$G_D$ [kPa]	$G_d$ [kPa]	$\eta_0$ [kPa s]	$\tau_d$ [s]	$J_e^0$ [kPa <sup>-1</sup> ]	$5G_d J_e^0$ [-]	$w_d$ [-]	$f_d^2$ [-]	SHI [-]	SHI <sub>exp</sub> [-]
PLA110	0.04	0	700	40	4.50	8.24	0.27	0.03	0.74	0.34	6.67	4.92	7
PLA160	0.04	0	600	90	2.97	12.7	0.75	0.06	0.88	0.18	13.8	12.1	12
PLA200	0.04	0.2	600	150	2.22	16.9	1.33	0.08	0.88	0.12	20.2	17.7	20
PLA320	0.04	0.3	610	180	1.03	29.0	5.18	0.18	0.92	$7.6 \times 10^{-2}$	33.2	30.4	33
PLA420	0.04	0.4	560	250	0.50	13.5*	4.89*	0.36	0.91	$4.5 \times 10^{-2}$	56.0	50.7	57

\* $T = 110^\circ\text{C}$ **Fig. 10** Normalized maximal elongational viscosity  $\eta_{E,\max}/\eta_0$  as a function of Weissenberg number  $Wi_d = \dot{\epsilon}\tau_d$  for several LDPE melts. Lines are calculated by the HMMSF model. Symbols indicate the calculated values at the experimental strain rates

at lower Weissenberg numbers  $Wi_d$  in comparison to the PS combs. The values of SHI<sub>m</sub> of the three LDPEs are well below that of the PS comb with 30 branches, while the strain hardening of LDPE C with SHI<sub>m</sub> = 20 is similar to that of comb 290 k-14-44 k with SHI<sub>m</sub> = 19. As shown in Fig. 12, the maximal elongational viscosity  $\eta_{E,\max}/\eta_0(Wi_d)$  of LDPE C is also similar to that of two PS model pom-poms with  $M_{w,b} = 100$  kg/mol,  $q_a = 12$ , and  $M_{w,a} = 24$  and 40 kg/mol, respectively. Again, Figs. 11 and 12 show that comparison of the strain hardening potential is possible across different chemistries and different topologies, if strain hardening assessment is based on the normalized elongational viscosity  $\eta_{E,\max}/\eta_0$  and the strain hardening index (SHI).

## Discussion and Conclusions

We have quantified the strain hardening potential of different polymer systems by considering the maximal value of the normalized elongational viscosity  $\eta_{E,\max}(Wi_d)/\eta_0$ , i.e., the normalized steady-state elongational viscosity or the normalized maximal elongational viscosity reached in the case of fracture or tensile stress overshoot, as a function of Weissenberg number  $Wi_d = \dot{\epsilon}\tau_d$ . We found that  $\eta_{E,\max}(Wi_d)/\eta_0$  reaches a maximal value at  $Wi_d \approx 2 - 8$ , and we showed that this maximal value of  $\eta_{E,\max}/\eta_0 = \text{SHI}_m$  can be used to assess

**Table 9** Characteristics of LDPEs: dilution modulus  $G_D$ , relaxation modulus  $G_d$ , zero-shear viscosity  $\eta_0$ , disengagement time  $\tau_d$ , steady-state compliance  $J_e^0$ , diluted fraction  $w_d$ , square of representa-tive stretch  $f_d^2$ , strain hardening index (SHI) (Eq. (16)), and observed strain hardening index (SHI<sub>m</sub>) for LDPE melts at measurement temperatures  $T$ 

LDPE	$G_D$ [kPa]	$G_d$ [kPa]	$T$ [°C]	$\eta_0$ [kPa s]	$\tau_d$ [s]	$J_e^0$ [kPa <sup>-1</sup> ]	$5G_d J_e^0$ [-]	$w_d$ [-]	$f_d^2$ [-]	SHI [-]	SHI <sub>m</sub> [-]
LDPE A	30	0.170	150	31.4	22.1	0.70	0.61	$7.5 \times 10^{-2}$	29.7	17.8	20
LDPE B	30	0.049	150	7.07	14.0	1.98	0.49	$4.0 \times 10^{-2}$	55.3	26.9	30
LDPE C	30	0.012	150	22.0	26.7	1.22	0.71	$6.2 \times 10^{-2}$	35.9	25.4	27
Dow 150R	10	0.084	160	379	581	1.53	0.64	$9.1 \times 10^{-2}$	24.4	15.7	18
1810H-V	10	0.018	150	36.2	25.9	0.72	0.65	0.13	16.7	10.8	14
3020D	5	0.239	130	978	637	0.65	0.78	0.22	10.2	7.95	9

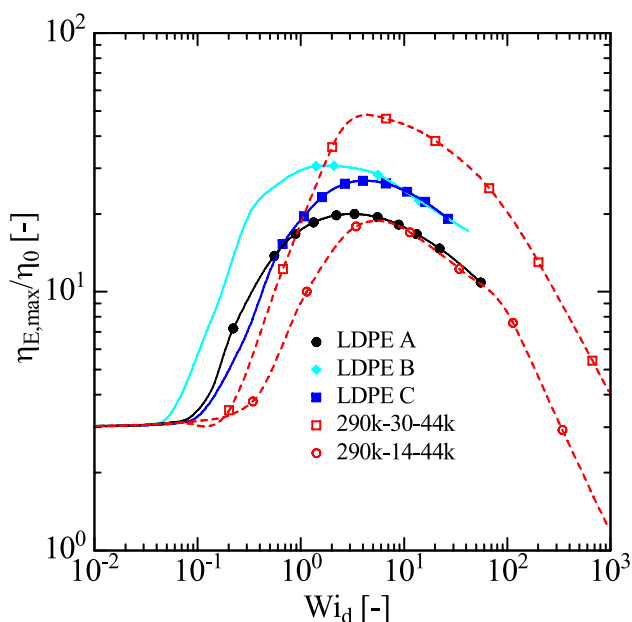


**Fig. 11** Comparison of normalized maximal elongational viscosity  $\eta_{E,max}/\eta_0(Wi_d)$  of LDPE A, B, and C, and PS combs 290 k-30-44 k and 290 k-14-44 k

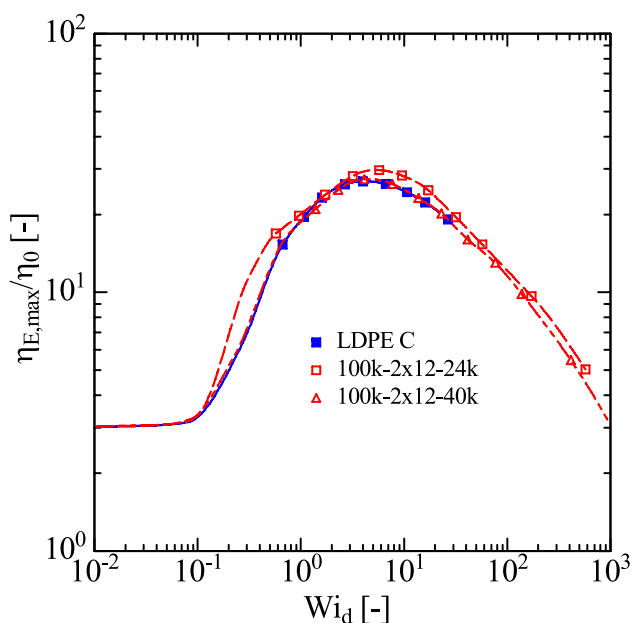


**Fig. 12** Comparison of normalized maximal elongational viscosity  $\eta_{E,max}/\eta_0(Wi_d)$  of LDPE C and PS model pom-poms with  $M_{w,b}=100$  kg/mol,  $q_a=12$ , and  $M_{w,a}=24$  and 40 kg/mol

the strain hardening behavior and to compare strain hardening of polymer melts across different topologies and different chemistries.  $SHI_m$  is the measured or observed strain hardening index. From a one-mode HMMSF model, we derived the strain hardening index  $SHI = 5f_d^2 G_d J_s^0$  (Eq. (16)),

which shows the same tendency as the experimentally observed  $SHI_m$  and is in nearly quantitative agreement with  $SHI_m$  up to  $SHI \approx 100$ , while at higher  $SHI$ ,  $SHI_m > SHI$ . Interestingly, the LVE factor  $5G_d J_s^0$  with  $G_d = G(t = \tau_d)$  is of order 1 for all polymer systems considered. This is a new result which deserves further investigation. The square of the characteristic stretch depends on hierarchical relaxation and dilution and is given by  $f_d^2 = \frac{1}{w_d} \sqrt{5(1+k)}$  (Eq. (14)) with the diluted polymer fraction  $w_d = (G_d/G_D)^{1/2}$  (Eq. (12)). Polymers systems with a large value of the steady-state compliance  $J_s^0$ , i.e., with a rather broad relaxation time spectrum and therefore a low value of  $G_d$ , show a high level of dynamic dilution resulting in a small polymer fraction  $w_d$  and consequently a large value of the characteristic stretch  $f_d$ , and therefore a large value of the strain hardening index ( $SHI$ ). This explains the conjecture of Mnstedt and Laun (1981) that the steady-state compliance  $J_s^0$  is correlated with strain hardening of long-chain branched polymers.

The strain hardening of PS combs with the same length of backbone and side chains increases with increasing number  $N_{br}$  of side chains, with the highest  $SHI \approx 200$  for the combs with the highest number of branches of  $N_{br} = 100\text{--}120$ , investigated corresponding to 5–6 side chains per entanglement length of the PS backbone. At the same number of side chains ( $N_{br} = 100$ ) and the same backbone length, shorter side chains with  $M_{w,a} = 15$  kg/mol lead to a much lower  $SHI$  than longer side chains with  $M_{w,a} = 40$  kg/mol, but binary blends of 10 or 20% of comb 310 k-100-15 k and 90 or 80% of linear PS 43 k, respectively, show the same  $SHI$  as comb 310 k-100-40 k. Pom-poms and combs with a similar number  $2q_a \approx N_{br}$  of side arms and side chains have similar strain hardening potential, but in contrast to combs with more than one side chain per entanglement length of the backbone, pom-poms do not show hyperstretching. From the comparison of the  $SHI$  of PS pom-poms and LDPE melts considered here, we may conclude that the strain hardening potential of a typical LDPE such as LDPE C ( $SHI = 25$ ) is equivalent to that of a pom-pom consisting of a backbone (largely independent of its length) and  $2q_a = 24$  side arms with a length corresponding to 2 to 3 times the entanglement molecular weight  $M_e$ . The strain hardening of LDPE A ( $SHI = 18$ ) is comparable to that of comb PS290k-14-44 k ( $SHI = 19$ ) having  $N_{br} = 14$  side chains with a molecular weight of 3 times  $M_e$ . Further research will be needed to confirm and extend these correlations across topologies and chemistries, which may allow rheologically guided topological tailoring of the strain hardening of industrially relevant long-chain branched polymers such as LDPE.

**Funding** Open Access funding enabled and organized by Projekt DEAL.

## Declarations

**Competing interests** The authors declare no competing interests.

**Open Access** This article is licensed under a Creative Commons Attribution 4.0 International License, which permits use, sharing, adaptation, distribution and reproduction in any medium or format, as long as you give appropriate credit to the original author(s) and the source, provide a link to the Creative Commons licence, and indicate if changes were made. The images or other third party material in this article are included in the article's Creative Commons licence, unless indicated otherwise in a credit line to the material. If material is not included in the article's Creative Commons licence and your intended use is not permitted by statutory regulation or exceeds the permitted use, you will need to obtain permission directly from the copyright holder. To view a copy of this licence, visit <http://creativecommons.org/licenses/by/4.0/>.

## References


- Abbasi M, Faust L, Riazi K, Wilhelm M (2017) Linear and extensional rheology of model branched polystyrenes: from loosely grafted combs to bottlebrushes. *Macromolecules* 50:5964–5977. <https://doi.org/10.1021/acs.macromol.7b01034>
- Abbasi M, Faust L, Wilhelm M (2019) Comb and bottlebrush polymers with superior rheological and mechanical properties. *Adv Mater* 31:e1806484. <https://doi.org/10.1002/adma.201806484>
- Dealy JM, Read DJ, Larson RG (2018) Structure and rheology of molten polymers: from structure to flow behavior and back again. Carl Hanser Verlag, Munich
- Doi M, Edwards SF (1979) Dynamics of concentrated polymer systems. Part 4.—Rheological properties. *J Chem Soc, Faraday Trans 2: Mol Chem Phys* 75:38–54. <https://doi.org/10.1039/F29797500038>
- Doi MF, Edwards S (1978) Dynamics of concentrated polymer systems. Part 1.—Brownian motion in the equilibrium state. *J Chem Soc, Faraday Trans 2: Mol Chem Phys* 74:1789–1801. <https://doi.org/10.1039/F29787401789>
- Faust L, Röpert M, Esfahani MK et al (2023) Comb and branch-on-branch model polystyrenes with exceptionally high strain hardening factor SHF=1000 and their impact on physical foaming. *Macromol Chem Phys* 224:2200214. <https://doi.org/10.1002/macp.202200214>
- Hepperle J, Münstedt H (2006) Rheological properties of branched polystyrenes: nonlinear shear and extensional behavior. *Rheol Acta* 45:717–727. <https://doi.org/10.1007/s00397-005-0031-9>
- Hirschberg V, Lyu S, Schußmann MG et al (2023) Modeling elongational viscosity of polystyrene pom-pom/linear and pom-pom/star blends. *Rheol Acta* 62:433–445. <https://doi.org/10.1007/s00397-023-01411-1>
- Hirschberg V, Schußmann MG, Röpert M-C et al (2023) Modeling elongational viscosity and brittle fracture of 10 polystyrene pom-poms by the hierarchical molecular stress function model. *Rheol Acta* 62:269–283. <https://doi.org/10.1007/s00397-023-01393-0>
- Hirschberg V, Faust L, Abbasi M et al (2024) Hyperstretching in elongational flow of densely grafted comb and branch-on-branch model polystyrenes. *J Rheol* 68:229–246. <https://doi.org/10.1122/8.0000781>
- Huang Q (2022) When polymer chains are highly aligned: a perspective on extensional rheology. *Macromolecules* 55:715–727. <https://doi.org/10.1021/acs.macromol.1c02262>
- Huang Q, Hassager O (2017) Polymer liquids fracture like solids. *Soft Matter* 13:3470–3474. <https://doi.org/10.1039/C7SM00126F>
- Huang Q, Alvarez NJ, Shabbir A, Hassager O (2016) Multiple cracks propagate simultaneously in polymer liquids in tension. *Phys Rev Lett* 117:087801. <https://doi.org/10.1103/PhysRevLett.117.087801>
- Kempf M, Barroso VC, Wilhelm M (2010) Anionic synthesis and rheological characterization of poly(p-methylstyrene) model comb architectures with a defined and very low degree of long chain branching. *Macromol Rapid Commun* 31:2140–2145. <https://doi.org/10.1002/marc.201000412>
- Kempf M, Ahirwal D, Cziep M, Wilhelm M (2013) Synthesis and linear and nonlinear melt rheology of well-defined comb architectures of PS and PpMS with a low and controlled degree of long-chain branching. *Macromolecules* 46:4978–4994. <https://doi.org/10.1021/ma302033g>
- Laun HM, Münstedt H (1978) Elongational behaviour of a low density polyethylene melt. *Rheol Acta* 17:415–425
- Lentzakis H, Vlassopoulos D, Read DJ et al (2013) Uniaxial extensional rheology of well-characterized comb polymers. *J Rheol* 57:605–625. <https://doi.org/10.1122/1.4789443>
- Münstedt H (2023) Various features of melt strain hardening of polymeric materials in uniaxial extension and their relation to molecular structure: review of experimental results and their interpretation. *Rheol Acta* 62:333–363. <https://doi.org/10.1007/s00397-023-01400-4>
- Münstedt H (2024) Melt strain hardening of polymeric systems increasing with decreasing elongational rate: experimental results and discussion of models. *Phys Fluids* 36:093120. <https://doi.org/10.1063/5.0227343>
- Münstedt H, Laun HM (1981) Elongational properties and molecular structure of polyethylene melts. *Rheol Acta* 20:211–221. <https://doi.org/10.1007/BF01678022>
- Narimissa E, Wagner MH (2016) From linear viscoelasticity to elongational flow of polydisperse linear and branched polymer melts: the hierarchical multi-mode molecular stress function model. *Polymer* 104:204–214. <https://doi.org/10.1016/j.polymer.2016.06.005>
- Narimissa E, Wagner MH (2019) Review of the hierarchical multi-mode molecular stress function model for broadly distributed linear and LCB polymer melts. *Polym Eng Sci* 59:573–583. <https://doi.org/10.1002/pen.24972>
- Narimissa E, Wagner MH (2019) Review on tube model based constitutive equations for polydisperse linear and long-chain branched polymer melts. *J Rheol* 63:361–375. <https://doi.org/10.1122/1.5064642>
- Narimissa E, Rolón-Garrido VH, Wagner MH (2015) A hierarchical multi-mode MSF model for long-chain branched polymer melts part I: elongational flow. *Rheol Acta* 54:779–791. <https://doi.org/10.1007/s00397-015-0879-2>
- Nielsen JK, Rasmussen HK, Denberg M et al (2006) Nonlinear branch-point dynamics of multiarm polystyrene. *Macromolecules* 39:8844–8853. <https://doi.org/10.1021/ma061476r>
- Poh L, Narimissa E, Wagner MH, Winter HH (2022) Interactive shear and extensional rheology—25 years of IRIS Software. *Rheol Acta* 61:259–269. <https://doi.org/10.1007/s00397-022-01331-6>
- Poh L, Wu Q, Pan Z et al (2023) Fracture in elongational flow of two low-density polyethylene melts. *Rheol Acta* 62:317–331. <https://doi.org/10.1007/s00397-023-01392-1>
- Schußmann MG, Kreutzer L, Hirschberg V (2024) Fast and scalable synthetic route to densely grafted, branched polystyrenes and polydienes via anionic polymerization utilizing P2VP as branching point. *Macromol Rapid Commun* 45:2300674. <https://doi.org/10.1002/marc.202300674>
- Schußmann MG, Wilhelm M, Hirschberg V (2024) Predicting maximum strain hardening factor in elongational flow of branched pom-pom polymers from polymer architecture. *Nat Commun* 15:3545. <https://doi.org/10.1038/s41467-024-47782-8>



- Wagner MH, Hirschberg V (2023) Experimental validation of the hierarchical multi-mode molecular stress function model in elongational flow of long-chain branched polymer melts. *J Nonnewton Fluid Mech* 321:105130. <https://doi.org/10.1016/j.jnnfm.2023.105130>
- Wagner MH, Hirschberg V (2024) Rheology of Poly( $\alpha$ -olefin) Bottlebrushes: effect of self-dilution by alkane side chains. *Macromolecules* 2110–2118:2110. <https://doi.org/10.1021/acs.macromol.3c02430>
- Wagner MH, Bastian H, Bernnat A et al (2002) Determination of elongational viscosity of polymer melts by RME and Rheotens experiments. *Rheol Acta* 41:316–325. <https://doi.org/10.1007/s00397-002-0228-0>
- Wagner MH, Hepperle J, Münstedt H (2004) Relating rheology and molecular structure of model branched polystyrene melts by molecular stress function theory. *J Rheol* 48:489–503. <https://doi.org/10.1122/1.1687786>
- Wagner MH, Narimissa E, Huang Q (2021) Scaling relations for brittle fracture of entangled polystyrene melts and solutions in elongational flow. *J Rheol* 65:311–324. <https://doi.org/10.1122/8.0000184>
- Wagner MH, Narimissa E, Poh L, Huang Q (2022) Modelling elongational viscosity overshoot and brittle fracture of low-density polyethylene melts. *Rheol Acta* 61:281–298. <https://doi.org/10.1007/s00397-022-01328-1>
- Wagner MH, Zografos A, Hirschberg V (2024) Modeling elongational rheology of model poly( $\pm$ )-lactide graft copolymer bottlebrushes. *J Nonnewton Fluid Mech* 327:105220. <https://doi.org/10.1016/j.jnnfm.2024.105220>
- Zografos A, All HA, Chang AB et al (2023) Star-to-bottlebrush transition in extensional and shear deformation of unentangled polymer melts. *Macromolecules* 2406–2417:2406. <https://doi.org/10.1021/acs.macromol.3c00015>
- Zografos A, Maines EM, Hassler JF et al (2024) Preparation and characterization of H-shaped polylactide. *ACS Macro Letters* 695–702:695. <https://doi.org/10.1021/acsmacrolett.4c00217>

**Publisher's Note** Springer Nature remains neutral with regard to jurisdictional claims in published maps and institutional affiliations.

## Authors and Affiliations

Manfred H. Wagner<sup>1</sup> · Max G. Schußmann<sup>2</sup> · Manfred Wilhelm<sup>2</sup> · Valerian Hirschberg<sup>1,3</sup> 

✉ Valerian Hirschberg  
valerian.hirschberg@kit.edu

Manfred H. Wagner  
manfred.wagner@tu-berlin.de

<sup>1</sup> Institute of Chemical Technology and Polymer Chemistry, Karlsruhe Institute of Technology, Karlsruhe, Germany

<sup>2</sup> Polymer Engineering/Polymer Physics, Berlin Institute of Technology (TU Berlin), Ernst-Reuter-Platz 1, 10587 Berlin, Germany

<sup>3</sup> Institute for Technical Chemistry, Technical University Clausthal, Arnold-Sommerfeld-Str. 4, 38678 Clausthal-Zellerfeld, Germany